A Model for Bubble–Bubble and Bubble–Wall Interaction in Bubble Formation

Zongyuan Xiao and Reginald B. H. Tan
Dept. of Chemical and Biomolecular Engineering, National University of Singapore, Singapore 119260, Singapore

DOI 10.1002/aic.10644
Published online September 9, 2005 in Wiley InterScience (www.interscience.wiley.com).

A theoretical model for bubble formation at a submerged orifice has been developed, which takes into account the interaction between the column wall and the growing bubble at the orifice, as well as the interaction between subsequent bubbles formed and detached from the orifice. Experiments involving high-speed photography and bubble frequency measurements were carried out with different chamber volumes, column and orifice diameters, and gas flow. In particular, it was found that decreasing the column diameter (that is, increasing the bubble–wall interaction) led to increased bubble–bubble interaction, as evidenced by a greater tendency for pairing and multiple bubbling. Simulated results using the theoretical model agreed very well with experimental data. © 2005 American Institute of Chemical Engineers *AIChE J,* 52: 86–98, 2006
Keywords: bubble formation, bubble–bubble interaction, bubble–wall interaction, potential flow, wake pressure

Introduction

Bubble formation at a submerged orifice has been investigated experimentally and theoretically in the past decades. However, nearly all of the previous studies on bubble formation have not specifically taken into account the dimensions of the bubble column. It has generally been assumed that the bubble column diameter was very large compared with the orifice size and the wall effect could be neglected.

Collins[1] carried out a study of the influence of containing walls on the velocity of spherical-cap bubbles. The work was extended by Bhaga and Weber,[2] who also investigated the influence of wall proximity on wake size, external flow fields, bubble shape, and skirt behavior. Coutanceau and Thizon[3] investigated the wall effect on the bubble behavior in highly viscous liquids experimentally and theoretically. Generally, increasing the diameter ratio λ ($\lambda = d/d_c$, where d is bubble diameter and d_c is column diameter) was found to cause bubble elongation, a decrease in terminal velocity, a substantial reduction in the wake volume and the rate of fluid circulation within the wake, and a delay in the onset and waviness of skirts.

Raebiger and Vogelpohl[4,5] studied the vertical interactions between bubbles at the orifice and proposed a bubble formation model valid for a whole gas flow regime including bubbling and jetting. Ruzicka et al.[6,7] investigated the effect of bubble column dimensions on flow regime transition. Bubble columns of three different diameters (d_c = 0.14, 0.29, 0.40 m) and free plate area of 0.2% were used in the experiment. They found that increasing column size tended to cause transition from the homogeneous to the heterogeneous regime.

Numerous models have been proposed to simulate bubble formation. Davidson and Schüler[8] were among the first to develop spherical models for bubble formation with the application of potential theory and a virtual mass term. Kupferberg and Jameson[9,10] used potential flow theory to derive equations for the motion of a spherical growing bubble, its radial expansion, and the dynamic pressures involved in the bubbling system. They introduced a correction to the theory of Davidson and Schüler, to account for the presence of the flat plate surrounding the orifice, and the method of images was used to find the solution to Laplace's equation.

It is well known that the wake pressure behind a detached, rising bubble can influence the liquid flow field of the subse-

Correspondence concerning this article should be addressed to R. B. H. Tan at chetanbh@nus.edu.sg.

quent bubble.[11] This study aims (1) to investigate the wall effect of the bubble column on bubble formation at a single submerged orifice and (2) to model theoretically the bubble formation process by accounting for bubble–wall interaction by potential flow analysis and for bubble–bubble interaction by the liquid wake pressure.

The wall effect on bubble formation can be rigorously modeled by applying the boundary integral method coupled with the method of images, as shown in the Appendix. This rigorous model unfortunately does not account for bubble–bubble interaction and is therefore unable to distinguish between single and multiple bubble formation. In this article, we introduce an approximate modeling approach based on spherical bubbles, using Lamb's[12] spherical harmonic equation for rising and growing bubbles, coupled with the solution proposed by Zhang and Tan[11] for wake pressure to account for bubble–bubble interaction. The model development is presented in the next section.

Model Development

The physical system is shown in Figure 1 and the primary assumptions of the model are:

(1) The bubble is assumed to be initially hemispherical, grows at the horizontal orifice to attain a spherical shape during formation, and deforms into a spherical-cap bubble after detachment.

(2) The depth of liquid above the plate is sufficiently high, compared with the bubble diameter, so that it has no effect on bubble formation. Vertical infinity of the liquid column is also assumed.

(3) A detached and rising bubble is assumed to exert a wake pressure on the subsequent bubble forming at the orifice. However, a following bubble has no effect on velocity or shape of the preceding bubble and the distant effects are not considered.

(4) At a particular instant, the orifice experiences either upward gas flow (referred to as *bubbling*) or no flow (referred to as *waiting*). At any instant, the orifice shows only one of the above phases.

(5) The gas is an ideal, compressible gas following an adiabatic equation of state. The pressure within the bubble is assumed to be uniform.

(6) The viscosity of the liquid is assumed to be negligible and the flow is assumed to be irrotational.

(7) The liquid above the plate remains stagnant except the motion caused by bubble translation and rising.

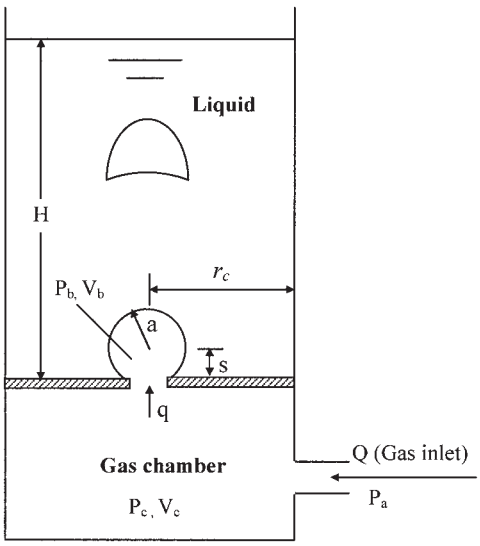

Figure 1. Physical system.

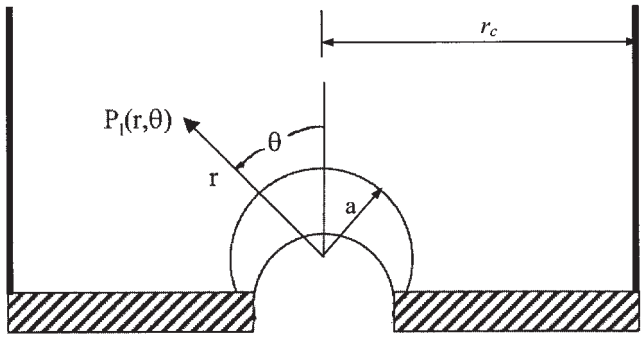

Figure 2. Growth of a bubble.

Analysis of the gas chamber pressure

The change of pressure in the gas chamber, P_c, is obtained by assuming an adiabatic process of ideal gas and applying the first law of thermodynamics to the gas chamber[13]

$$V_c \frac{dP_c}{dt} = \gamma P_c (Q - q) \tag{1}$$

where γ is the adiabatic exponent of the gas, V_c is the chamber volume, and Q and q are the volumetric gas flow into the chamber and through the orifice, respectively.

Orifice equation

Gas flow through the orifice is determined by the following orifice equation

$$\frac{dV_b}{dt} = k_o \sqrt{P_c - P_b} \tag{2}$$

where $k_o = \pi r_o^2 \sqrt{2/\rho_g C_g}$ is the orifice coefficient, $C_g = 1.5 + 2f'b/r_o$,[14] and f' is the fanning friction factor, which is approximated by $f' = 16/\mathrm{Re}_o$ ($\mathrm{Re}_o = 2\rho_g r_o u_o/\mu_g$, where u_o is instantaneous gas velocity through the orifice), if laminar flow is assumed; b is orifice plate thickness.

Liquid pressure analysis

The viscosity of the liquid is assumed to be negligible and the flow is assumed to be irrotational. Therefore the potential flow theory can be used to describe the process.

Because the bubble is assumed to be spherical, a moving spherical coordinate system is used, with the origin located at the center of the growing and translating bubble, as shown in Figure 2.

Lamb,[12] in his classic treatise on hydrodynamics, assumed the velocity potential for a spherical ball moving upward with velocity U (Article 93[12]) to be: $\phi_T = [Ar + (B/r^2)]\cos\theta$. In our

case of cylindrical vessel walls, we apply the appropriate boundary conditions [$-(\partial\phi/\partial r) = U\cos\theta$ when $r = a$; $-(\partial\phi/\partial r) = 0$ when $r = r_c/\sin\theta$], to obtain the following expression for the velocity potential

$$\phi_T = \left[\frac{a^3\sin^3\theta}{r_c^3 - a^3\sin^3\theta}\,Ur + \frac{a^3r_c^3}{2(r_c^3 - a^3\sin^3\theta)}\,\frac{U}{r^2}\right]\cos\theta \quad (3)$$

Similarly for spherical expansion, the spherical zonal harmonics takes the form $\phi_p = [Ar + (B/r)]\dot{a}$, and with the boundary conditions [$-(\partial\phi/\partial r) = \dot{a}$ when $r = a$; $-(\partial\phi/\partial r) = 0$ when $r = r_c/\sin\theta$)], the following velocity potential equation can be obtained

$$\phi_p = \left[\frac{a^2r_c^2}{r(r_c^2 - a^2\sin^2\theta)} + \frac{a^2r\sin^2\theta}{r_c^2 - a^2\sin^2\theta}\right]\dot{a} \quad (4)$$

where a is an instantaneous bubble radius, r_c is radius of the bubble column, U is the bubble rising velocity, r and θ are the coordinates from the bubble center, and the overdot denotes a time derivative.

The velocity potential ϕ around a spherical bubble that is expanding and rising can be expressed as the sum of the potential ϕ_T attributed to the rising motion and the potential ϕ_p associated with the expansion,[12,15] as follows

$$\phi = \phi_T + \phi_p = \left[\frac{a^3\sin^3\theta}{r_c^3 - a^3\sin^3\theta}\,Ur + \frac{a^3r_c^3}{2(r_c^3 - a^3\sin^3\theta)}\,\frac{U}{r^2}\right]\cos\theta + \left[\frac{a^2r_c^2}{r(r_c^2 - a^2\sin^2\theta)} + \frac{a^2r\sin^2\theta}{r_c^2 - a^2\sin^2\theta}\right]\dot{a} \quad (5)$$

During bubble formation, liquid pressure $P_l(r, \theta)$ can be expressed as the sum of hydrostatic pressure (P_{st}) at that point, the pressure arising from bubble expansion and translation, and the wake pressure arising from the preceding rising bubble. For a given liquid velocity distribution, Bernoulli's expression is

$$\frac{P_l(r,\theta) - P_{st} - P_w}{\rho_l} = \frac{\partial\phi}{\partial t} - \frac{1}{2}|u|^2 \quad (6)$$

where P_{st} and P_w represent hydrostatic pressure and wake pressure, respectively, at the coordinate (r, θ) and the absolute liquid velocity is

$$|u| = \sqrt{\left(\frac{\partial\phi}{r\partial\theta}\right)^2 + \left(\frac{\partial\phi}{\partial r}\right)^2} \quad (7)$$

Translation of the (r, θ) coordinate system at velocity U may be accounted for by using the two expressions

$$\dot{r} = -U\cos\theta \qquad \dot{\theta} = U\frac{\sin\theta}{r} \quad (8)$$

By substituting Eqs. 5 and 7 into Eq. 6, and with some simplification, we obtain

$$\begin{aligned}\frac{P_l(r,\theta) - P_{st} - P_w}{\rho_L} = {} & \frac{2a\dot{a}^2 + a^2\ddot{a}}{r} + \frac{5a^2\dot{a}U\cos\theta}{2r^2} + \frac{a^3\dot{U}\cos\theta}{2r^2} - \frac{a^3U^2\sin^2\theta}{2r^3} + \frac{a^3U^2\cos^2\theta}{r^3} \\ & - \frac{a^4\dot{a}^2}{2r^4} - \frac{a^5\dot{a}U}{r^5}\cos\theta - \frac{a^6U^2}{8r^6}\sin^2\theta - \frac{a^6U^2}{2r^6}\cos^2\theta \\ & + \frac{2a\dot{a}^2r\sin^2\theta + a^2\ddot{a}r\sin^2\theta + a^2\dot{a}U\sin^2\theta\cos\theta}{r_c^2} \\ & + \frac{3a^2\dot{a}Ur\sin^3\theta\cos\theta + a^3\dot{U}r\sin^3\theta\cos\theta + 2a^3U^2\sin^3\theta\cos^2\theta - a^3U^2\sin^5\theta}{r_c^3} \\ & + \left(\frac{a^2\dot{a}}{r^2} + \frac{a^3U\cos\theta}{r^3}\right)\left(\frac{a^2\dot{a}\sin^2\theta}{r_c^2} + \frac{a^3U\sin^3\theta\cos\theta}{r_c^3}\right) \\ & + \frac{a^3U\sin\theta}{2r^2}\left(\frac{a^2\dot{a}\sin^2\theta}{r_c^2} + \frac{a^3U\sin^3\theta\cos\theta}{r_c^3}\right)\end{aligned} \quad (9)$$

P_{or} can be found by substituting $\theta = \pi$, $r = s$:

$$P_{or} = \frac{\rho_l a^2\ddot{a}}{s} + \frac{\rho_l a\dot{a}^2}{s}\left(2 - \frac{a^3}{2s^3}\right) - \frac{\rho_l a^2\dot{a}\dot{s}}{s^2}\left(1 - \frac{a^3}{s^3}\right) + \frac{\rho_l a^3\dot{s}^2}{s^3}\left(1 - \frac{a^3}{2s^3}\right) - \frac{\rho_l g a^3}{s^2} + P_\infty + P_{wo} \quad (10)$$

where P_∞ is the static pressure at orifice and P_{wo} is wake pressure at the orifice.

Bubble pressure analysis

The pressure within the bubble P_b is assumed to be uniform and equal to the average pressure in the liquid at the bubble boundary ($\bar{P}_l$), plus the pressure arising from surface tension.

The average liquid pressure at the bubble boundary ($\bar{P}_l$) can be calculated by integrating the liquid pressure over the bubble surface as follows:

$$\bar{P}_l \int_{-s}^{a} 2\pi a dx = \int_0^{\theta'} [2\pi a \sin\theta P_l(r,\theta)a]_{r=a} d\theta \quad (11)$$

where $\theta' = \cos^{-1}(-s/a)$.

With some manipulation, we obtain

$$P_b = \rho_l\left(\frac{3}{2}\dot{a}^2 + a\ddot{a} - gs\right) - \frac{\rho_l U^2 a}{4(s+a)} \times \left(1 + \frac{5}{2}\frac{s}{a} - \frac{3s^3}{2a^3}\right) + \frac{\rho_l a}{a+s} \times \left[\frac{a^3\ddot{a}}{r_c^2}\left(\frac{2}{3} + \frac{s}{a} + \frac{s^3}{3a^3}\right) + \frac{a^2\dot{a}U + a^3\dot{a}U}{r_c^2} \times \left(\frac{1}{4} - \frac{s^2}{2a^2} + \frac{s^4}{4a^4}\right) + \frac{4a^3\dot{a}U + a^4\dot{U}}{5r_c^3a^5}(a^2 - s^2)^{5/2} + \frac{3a^2\dot{a}}{r_c^2}\left(\frac{2}{3} + \frac{s}{a} + \frac{s^3}{3a^3}\right)\right] + P_\infty + P_{wb} + \frac{2\sigma}{a} \quad (12)$$

where P_{wb} is the wake pressure imposed by the preceding bubble, which is discussed below.

Wake pressure analysis

The pressure field in the wake of a detached rising bubble will affect the growth of the next bubble. When the bubble detaches, a tongue of liquid moves upward into the rear of the bubble, so that the bubble immediately begins to deform toward a spherical-cap bubble and attains its terminal velocity.[16] With Oseen's modification to potential flow, the wake pressure, caused by the detached rising bubble with steady velocity at the orifice, can be written as follows[11,17]

$$P_{wo} = \frac{-6}{N_{\mathrm{Re}}}\left(\frac{\rho_l U_T^2}{2}\right)\frac{a_{sc}^2}{s_{bo}^2} - \frac{\rho_l U_T^2 a_{sc}^3}{2s_{bo}^3} \quad (13)$$

where a_{sc} is the cap radius of the rising spherical-cap bubble and U_T is the terminal rising velocity of the spherical-cap bubble, given by the expression of Davies–Taylor equation[16]

$$U_T = \frac{2}{3}\sqrt{\frac{g a_{sc}(\rho_l - \rho_g)}{\rho_l}} \quad (14)$$

where s_{bo} is the distance between the rising bubble and the orifice and N_{Re} ($=2a_{sc}U_T\rho_l/\mu_l$) is the Reynolds number of the detached rising bubble.

Similarly, the wake pressure at the bubble surface is expressed as follows

$$P_{wb} = \frac{-6}{N_{\mathrm{Re}}}\left(\frac{\rho_l U_T^2}{2}\right)\frac{a_{sc}^2}{s_{bb}^2} - \frac{\rho_l U_T^2 a_{sc}^3}{2s_{bb}^3} \quad (15)$$

where s_{bb} is the mean distance between the detached rising bubble and the growing bubble.

Force balance for the bubble

A force balance between the acceleration of added mass and buoyancy can be written as[18]

$$\frac{d}{dt}\left(\frac{11}{16}\rho_l V_b U\right) = (\rho_l - \rho_g)V_b g \quad (16)$$

The value 11/16 is the added mass coefficient of a sphere in the vicinity of a plane wall.[19]

Bubble detachment criteria

With the growth and translation of the bubble, detachment will be possible if the liquid pressure at the orifice P_{or} becomes greater than the bubble pressure P_b at the instant in time when $s = a$ (that is, the earliest time for detachment is when the bubble base is tangential to the orifice plate). If the orifice pressure P_{or} is also greater than the chamber pressure P_c, weeping is possible after bubble detachment. This situation is known as "true single bubbling."

However, the phenomenon of "pairing" or "multiple bubbling" will be possible if $P_{or} < P_c$ when $s = a$. Immediately after the bubble has detached at the point of $s = a$, there is an instantaneous upward pressure drop across the orifice because $P_c > P_{or}$. This pressure difference $P_c - P_{or}$ will cause a smaller second bubble to grow very quickly. When $s = a$, the second detaches and it catches up to and coalesces with the preceding bubble as a result of the upward wake pressure. The process repeats until P_c is not larger than P_{or} again. It is necessary at this stage to distinguish between "pairing" and "multiple bubbling," although the two are very similar in appearance. One simple definition could be used to distinguish them as follows: only two bubbles are formed during one cycle of bubble formation for "pairing," whereas more than two bubbles are formed during one cycle of bubble formation for "multiple bubbling."

The criteria for detachment can now be expressed as: the bubble detaches at $s = a$; "pairing" or "multiple bubbling" happens if $P_{or} < P_c$ when the bubble has detached, a smaller second or third bubble is formed immediately after the preceding detachment; the bubble formation period is ended when P_c is not larger than P_{or} and it enters into the waiting period of one cycle.

Chamber pressure during waiting period

After bubble detachment, the pressure in the chamber will accumulate as a consequence of the continuous input of gas but no outflow of gas from chamber. The chamber pressure expression during waiting time is obtained from Eq. 1 under the condition $q = 0$:

$$\ln P_c = \frac{\gamma}{V_c} QT + \ln P_{cDET} \tag{17}$$

where T is the time from the instant of bubble detachment and P_{cDET} is the chamber pressure at bubble detachment.

Bubble frequency f

One cycle of bubble formation consists of formation time and waiting time. The formation time t_f can be calculated with the model and the waiting time t_w can be calculated from Eq. 17. Thus the bubble formation period of one cycle is equivalent to the sum of t_f and t_w and the frequency of bubble formation f, which corresponds to the number of bubbles formed per unit time, is the inverse number of the period as follows

$$f = \frac{1}{t_f + t_w} \tag{18}$$

Numerical solution strategy

The expression for gas flow into a growing spherical bubble

$$q = \frac{dV_b}{dt} \tag{19}$$

and the definition of bubble rising velocity during formation

$$U = \frac{ds}{dt} \tag{20}$$

ensure closure of the system of equations describing bubble formation. Equations 1, 2, 12, 13, 15, 16, 19, and 20 can be solved simultaneously for the variables P_c, P_b, P_{wb}, P_{wo}, q, a, s, and U using a standard Runge–Kutta–Verner fifth- and sixth-order method.

The initial conditions were $P_c(0) = P_b(0) = P_\infty + (2\sigma/r_o) + P_{wo}(0)$, $q(0) = U(0) = s(0) = 0$, and $a = r_o$, corresponding to a hemisphere with radius equal to the orifice radius.

The simulations were carried out for a chain of bubbles. The initial bubble was allowed to form in a quiescent liquid, that is, it experienced no wake effect. Each subsequent bubble was then simulated as forming, detaching, and rising under the influence of the wake pressure of its immediate predecessor. In most cases, straightforward convergence was attained at the third cycle of bubble formation, that is, the second and the third cycle of bubble formation were virtually identical. The converged values of waiting time and formation time then constitute one bubbling cycle.

Experimental Work

Figure 3 shows the experimental apparatus, which consisted of a cylinder as the bubble column, a plate insert, and a cylinder as the gas chamber. Purified air ($\gamma = 1.4$) from the compressed gas cylinder was introduced into the gas chamber. Air flow was controlled by means of three gas flow meters with various ranges. A high-speed video camera was used to visually observe bubble formation and a pressure transducer was used to record pressure fluctuations in the gas chamber.

The bubble column, designed conveniently for visual and photographical observations, was located above the plate insert and

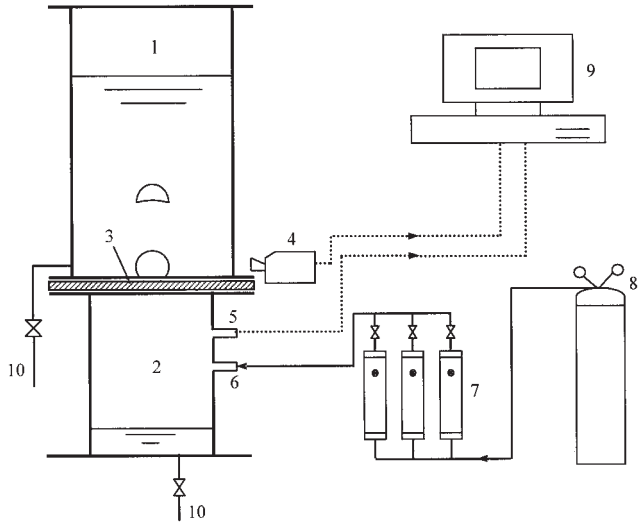

Figure 3. Experimental setup.

Legend: 1: bubble column; 2: gas chamber; 3: plate insert; 4: high-speed camera; 5: pressure transducer; 6: gas inlet; 7: gas flow meters; 8: gas cylinder; 9: read-out computer; 10: drain.

gas chamber. The cylindrical bubble column was made of Plexiglas® (5 mm thick). To investigate the effect of column wall on bubble formation, three sizes of column ($ID\phi$ 30 × 470 mm, $ID\phi$ 50 × 470 mm, and $ID\phi$ 100 × 470 mm) were designed. The column was open to the atmosphere at the top and from which water was introduced into the column. A drain valve was designed near the bottom of the column to remove the liquid.

The gas chamber, also made of Plexiglas® (5 mm thick), was located right below the plate insert. Two cylindrical gas chambers with different dimensions ($ID\phi$ 60 × 300 mm and $ID\phi$ 100 × 300 mm), were used during the experiment to achieve different gas chamber volumes. The volume of the gas chamber could be varied from 260 to 2000 cm^3 by filling it partially with water. A drain valve was placed at the bottom of the gas chamber to remove the liquid.

An interchangeable plate insert allowed various sizes of orifice to be investigated. Three sizes of orifices with diameters of 1.6, 2.0, and 2.4 mm, respectively, were designed.

The gas supply system consisted of a high-pressure gas cylinder, pressure regulator, rotameters, and other ancillary apparatus. Purified air from the compressed gas cylinder was introduced into the gas chamber. Three rotameters (Keiso, Tokyo, Japan), covering the range of gas flow 0.08–0.83, 0.5–5.0, and 3.3–33 cm^3/s, respectively, were connected in parallel to control the gas flow into the gas chamber. To ensure a smooth flow, the upstream pressure was maintained at a value higher than that of the chamber pressure.

Pressure fluctuations during bubble formation in the gas chamber were recorded by Microphone ICP® Pressure Sensor (Model 106B50, PCB Piezotronics). The analog output from the signal conditioner was fed into the computer through a 12-bit ADC (analog digital converter, Pico). The ADC-12 converter was connected to the printer port of a computer. Its measurement range was between 0 and 5 V. Collected data were analyzed by a driving software installed in the computer. Bubble frequencies were determined by Fourier transform of the pressure–time series data.

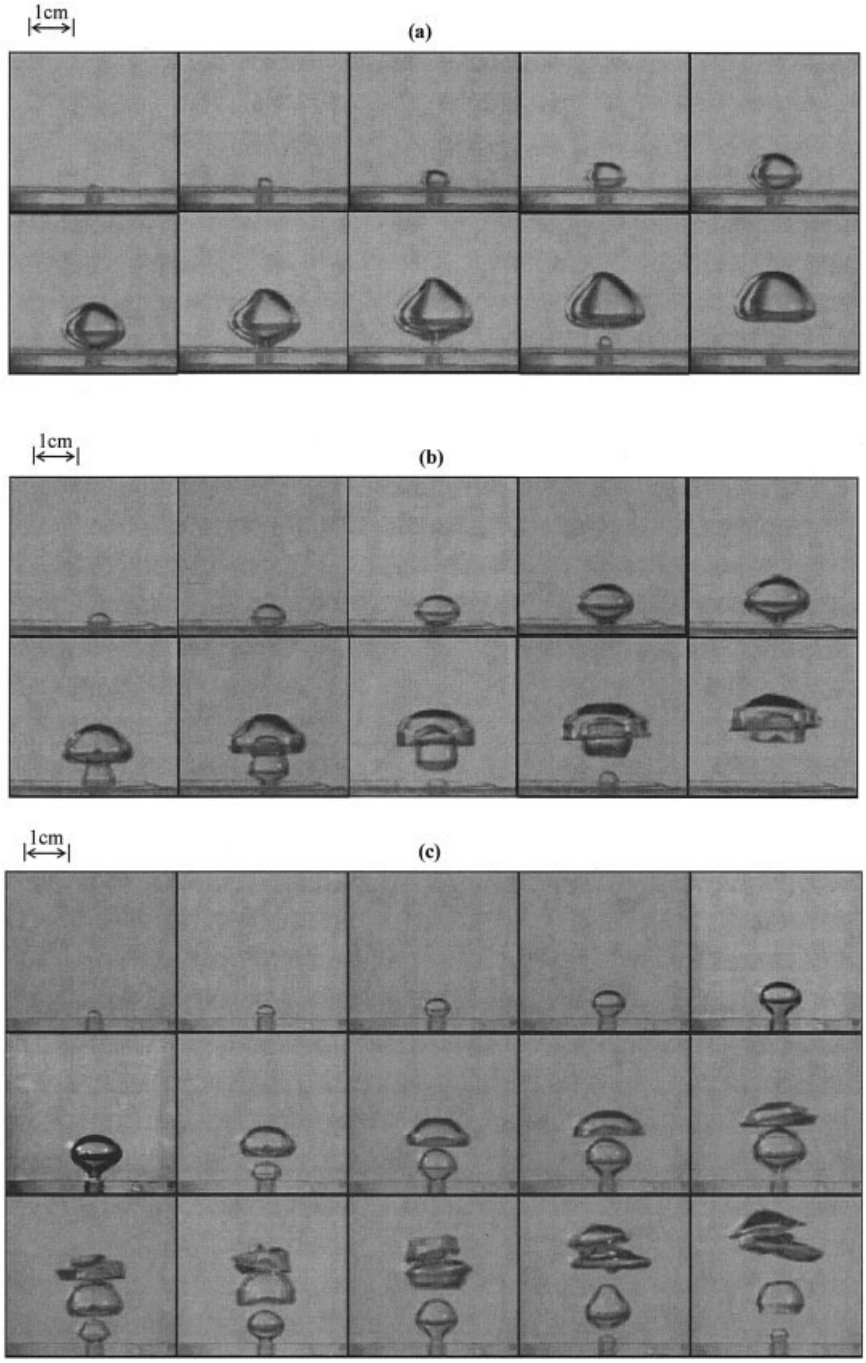

Figure 4. High-speed video pictures at $Q = 0.854$ cm^3/s, $d_o = 2.4$ mm, and $V_c = 430$ cm^3.

(a) $d_c = 100$ mm, time interval = 6 ms; (b) $d_c = 50$ mm, time interval = 8 ms; (c) $d_c = 30$ mm, time interval = 8 ms.

High-speed images were recorded during the experiments to verify the link between pressure transducer fluctuations and actual physical dynamics of the system. The Photron™ FASTCAM-PCI high-speed video camera system, used for this purpose, was composed of a FASTCAM-PCI camera head, a zoom lens, and a control PCI board connecting with the computer. The key features of the system were 500 full frames recorded at 512 × 480 resolution per second and an analysis software (MotionPlus) was installed in the computer to create image files.

To confirm the reliability of the experimental results and maximize the accuracy of the experiment, most of the experiments were done in triplicate.

Results and Discussion

Effect of the column diameter

The wall effect on bubble formation was investigated through the change of the column size. Figures 4a to 4c shows the video sequences of bubble formation for various column diameters of 100, 50, and 30 mm, respectively. The other

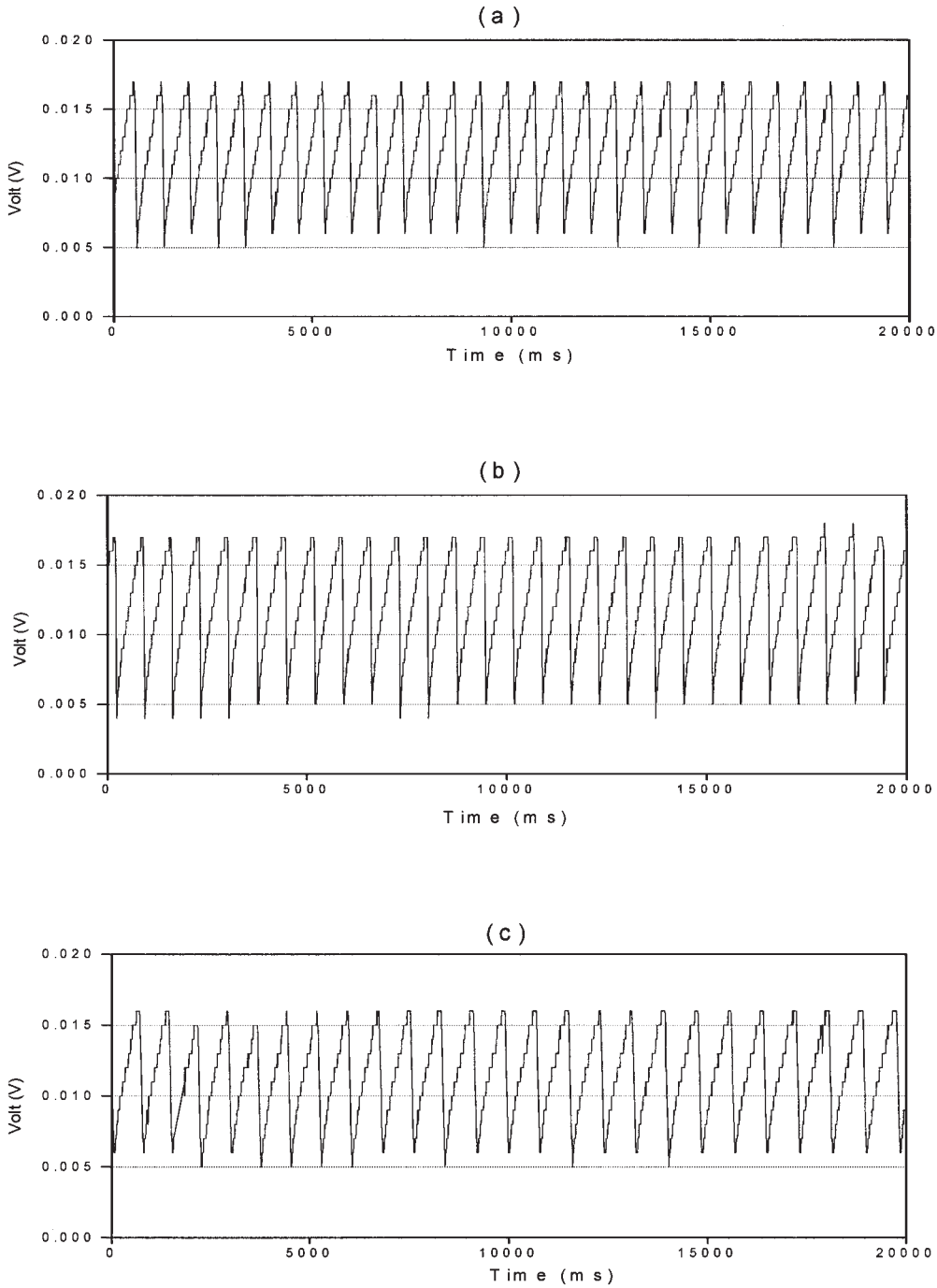

Figure 5. Typical pressure signals at d_o = 2.4 mm, Q = 0.854 cm^3/s, and V_c = 430 cm^3 with several column diameters.

(a) d_c = 100 mm; (b) d_c = 50 mm; (c) d_c = 30 mm.

parameters are kept constant for these three sets of experiments as follows: gas flow Q = 0.854 cm^3/s, chamber volume V_c = 430 cm^3, the orifice diameter d_o = 2.4 mm, and the liquid height H = 30 cm. It can be observed from these video sequences that bubbles attain the typical spherical-cap shape soon after detachment. The corresponding chamber pressure signal and the Fast Fourier Transform (FFT) analysis of the pressure signals are shown in Figures 5 and 6 respectively.

It is observed that for the largest column with diameter d_c = 100 mm, only one single bubble is formed for each cycle and when the bubble detaches, the process enters into the waiting period until the next cycle starts, that is, single bubbling is clearly observed. The bubble formation frequency is highest among these three cases. When d_c = 50 mm, it is found that when the first bubble detaches, a smaller second bubble is formed immediately and the second bubble catches up to and coalesces with the first one. After the second bubble detaches, the process enters into the waiting period until the next cycle

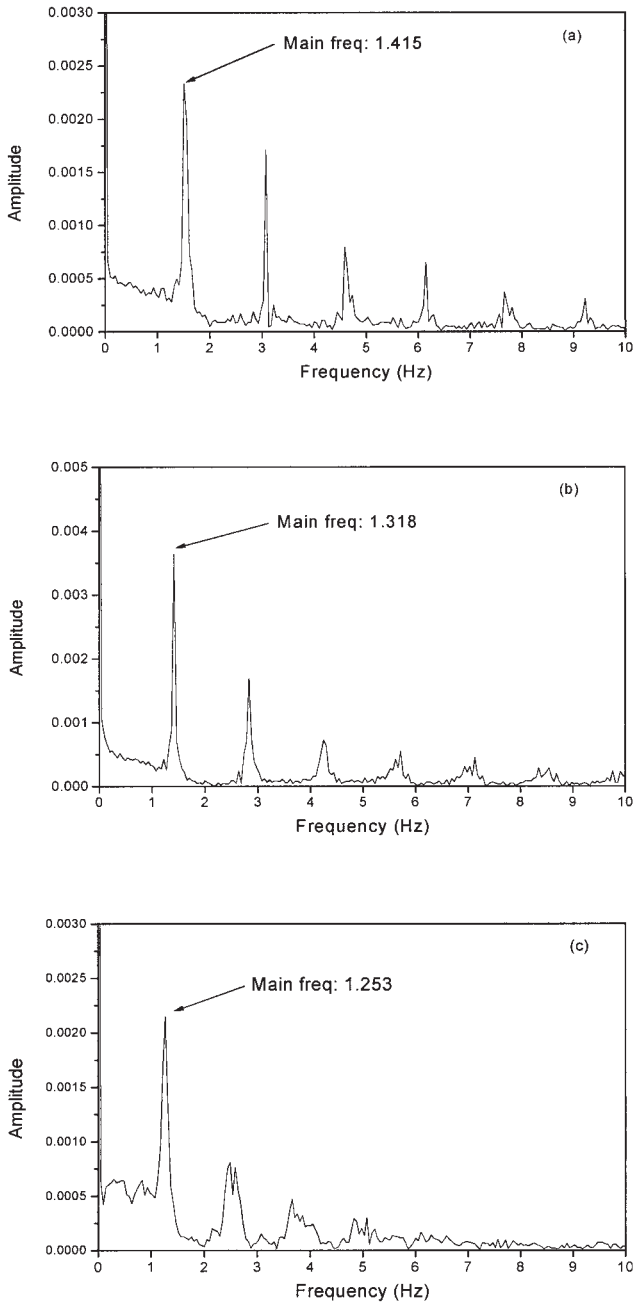

Figure 6. Signal spectrum at d_o = 2.4 mm, Q = 0.854 cm^3/s, and V_c = 430 cm^3 with several column diameters.

(a) d_c = 100 mm; (b) d_c = 50 mm; (c) d_c = 30 mm.

starts; we can classify this as pairing. The bubble formation frequency is smaller compared with the case of d_c = 100 mm. When d_c = 30 mm, it is found that when the first bubble detaches, a smaller second bubble is formed immediately and when the second detaches, a smaller third bubble is formed immediately and the second and third bubbles catch up to and coalesce with the first one. After the third bubble detaches, the process enters into the waiting period until the next cycle starts; this is a case of multiple bubbling. The bubble formation frequency is the smallest among these three cases. Typical values of Reynolds number (Re), Weber number (We), and Morton number (Mo) for the detached bubbles shown in Figure 4 are N_{Re} = 500–900, We = 50, and Mo = 10^{-7}.

It is very interesting that by decreasing the column diameter, with all other conditions remaining unchanged, the regime of the bubble formation changes from single bubbling to pairing and eventually multiple bubbling, indicating that increasing bubble–wall interaction leads to increased bubble–bubble interaction.

Effect of the gas chamber volume

The effect of chamber volume on bubble formation was investigated by varying the chamber volume from 430 to 1000 cm^3 while keeping other operation conditions constant, that is, gas flow Q = 0.854 cm^3/s, orifice diameter d_o = 2.4 mm, and liquid height H = 30 cm for three sizes of column. The video sequences of bubble formation with V_c = 1000 cm^3 for column diameters of 100, 50, and 30 mm are shown in Figures 7a to 7c, respectively.

It can be observed from Figure 7a that for d_c = 100 mm, a smaller second bubble is formed immediately after the first detaches and the second one catches up to and coalesces with the first one. After the second bubble detaches, the process enters into the waiting period until the next cycle starts. Compared with the case of single bubbling with chamber volume V_c = 430 cm^3 (Figure 4a), the larger chamber volume has clearly shifted the bubble formation into the pairing regime. For d_c values of 50 and 30 mm, the bubble formation for V_c = 1000 cm^3 is clearly within the multiple bubbling regime, that is, three or more bubbles are formed in rapid succession during each bubbling cycle. Overall, the bubbling frequency is lower for V_c = 1000 cm^3 compared with the smaller chamber volume.

The results show that with increasing chamber volume, the regime of the bubble formation will shift toward pairing and multiple bubbling, with a consequent decrease in bubbling frequency. This observation is consistent with the conclusion reported by McCann and Prince[20] that pairing and multiple bubbling were more likely to occur in the case of large chamber volumes.

Comparison of experimental results with theoretical predictions

The validity of our theoretical model was investigated by comparing simulated results of bubbling frequency with a wide range of experimental data for various column and orifice diameters, chamber volumes, and gas flow.

Figure 8a shows the relationship between bubbling frequency and gas flow for three sizes of column with orifice diameter d_o = 1.6 mm and chamber volume V_c = 430 cm^3. The comparisons of experimental results with theoretical predictions are also shown in this figure. When orifice diameters are changed to 2.0 and 2.4 mm, the corresponding relationships are shown in Figures 8b and 8c, respectively. The experimental trends are very clear: bubbling frequency increases with increasing column diameter and also with increasing gas flow, whereas bubbling frequency decreases with increasing orifice diameter. Our theoretical model predicts these trends very well, and the agreement between simulated and experimental frequencies is very good.

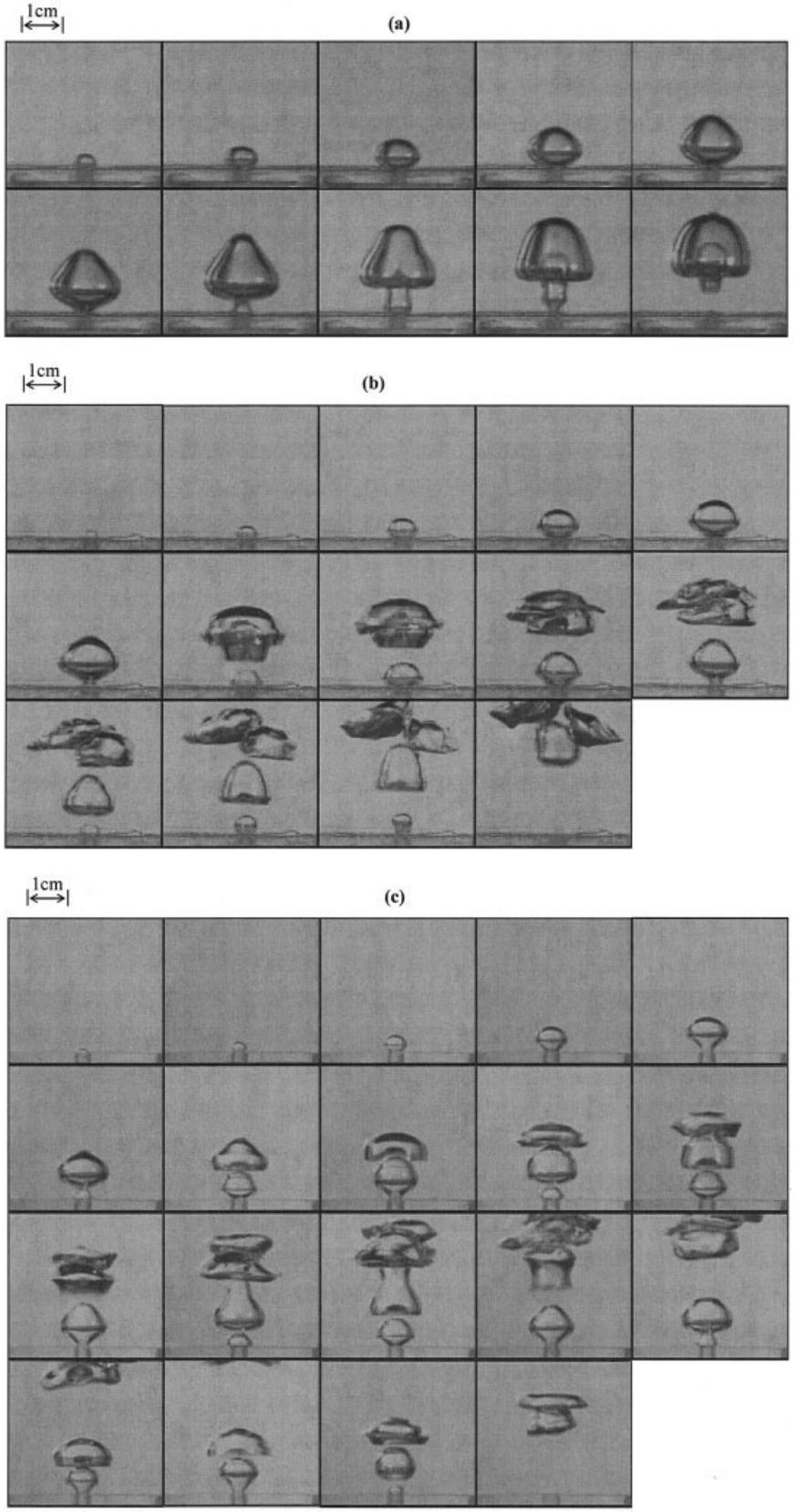

Figure 7. High-speed video pictures at Q = 0.854 cm^3/s, d_o = 2.4 mm, and V_c =1000 cm^3.

(a) d_c = 100 mm, time interval = 6 ms; (b) d_c = 50 mm, time interval = 8 ms; (c) d_c = 30 mm, time interval = 10 ms.

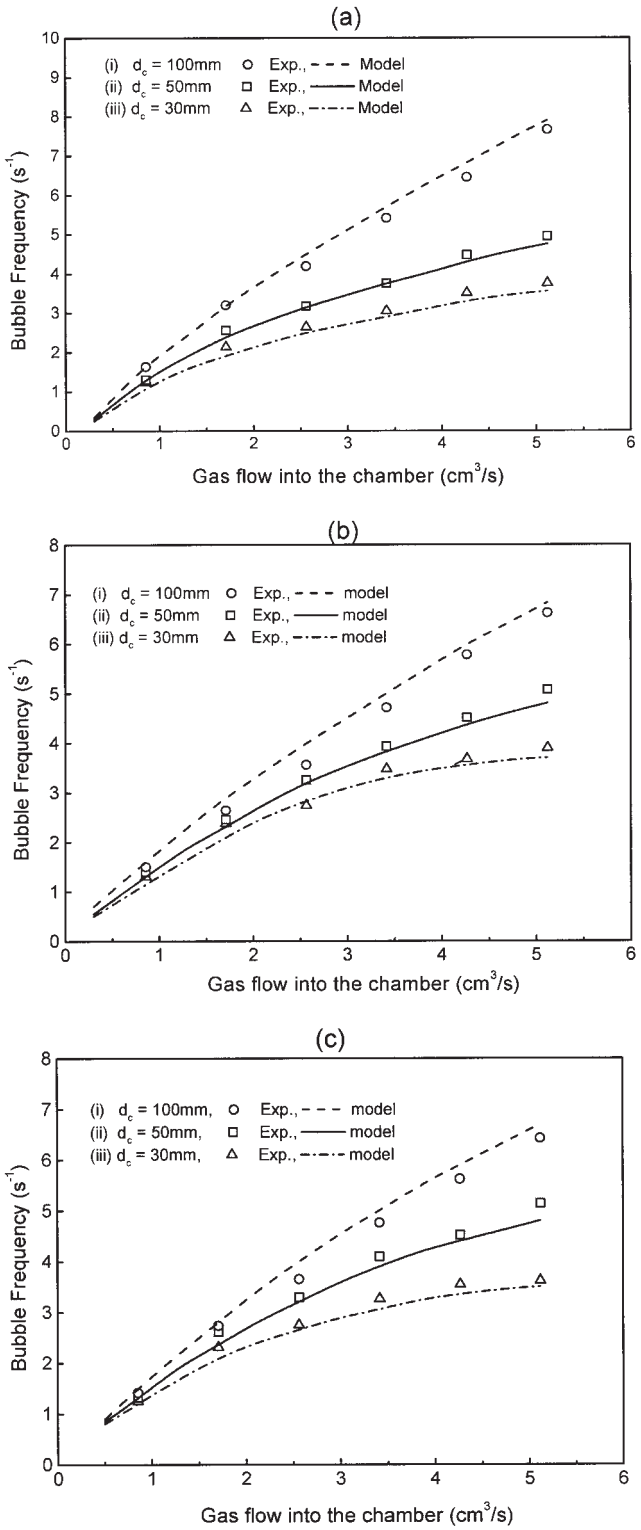

Figure 8. Relationship between bubble frequency and gas flow for various column diameters (i) d_c = 100 mm (ii) d_c = 50 mm (iii) d_c = 30 mm at V_c = 430 cm^3: (a) d_o = 1.6 mm; (b) d_o = 2.0 mm; (c) d_o = 2.4 mm.

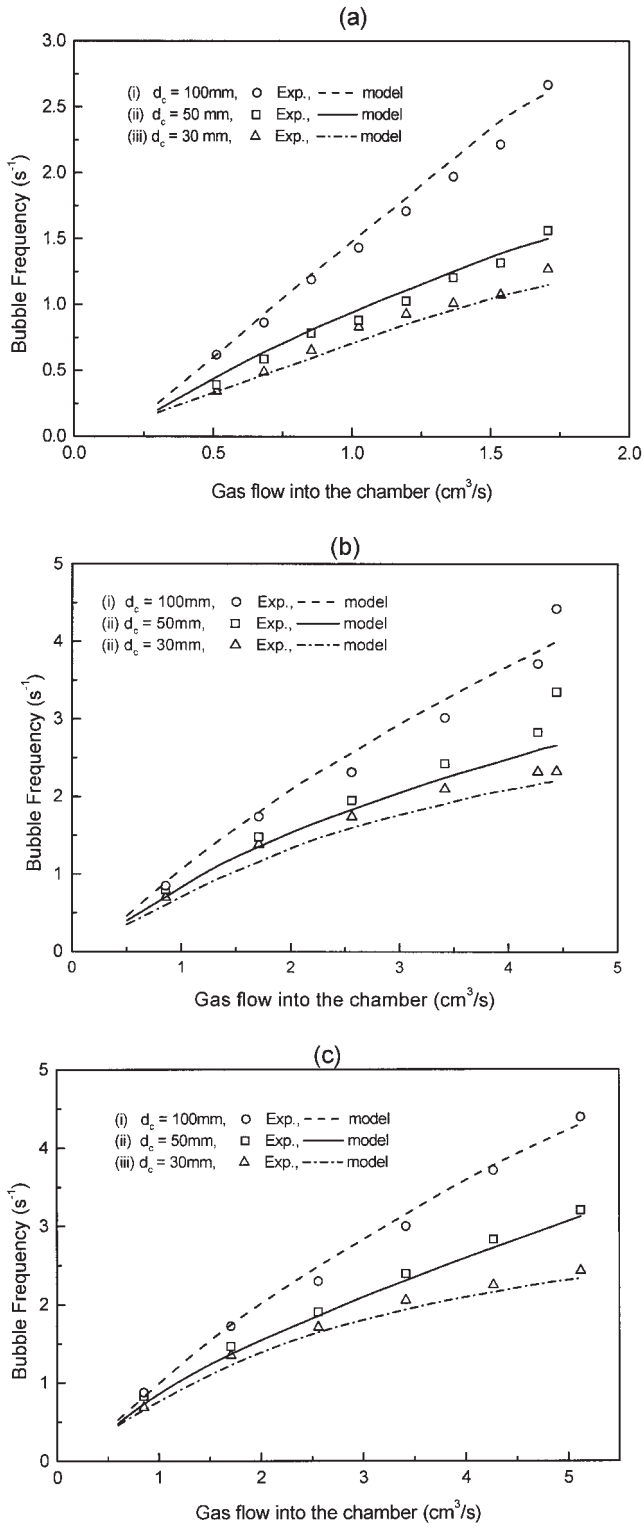

Figure 9. Relationship between bubble frequency and gas flow for various column diameters: (i) d_c = 100 mm; (ii) d_c = 50 mm; (iii) d_c = 30 mm at V_c = 1000 cm^3.

(a) d_o = 1.6 mm; (b) d_o = 2.0 mm; (c) d_o = 2.4 mm.

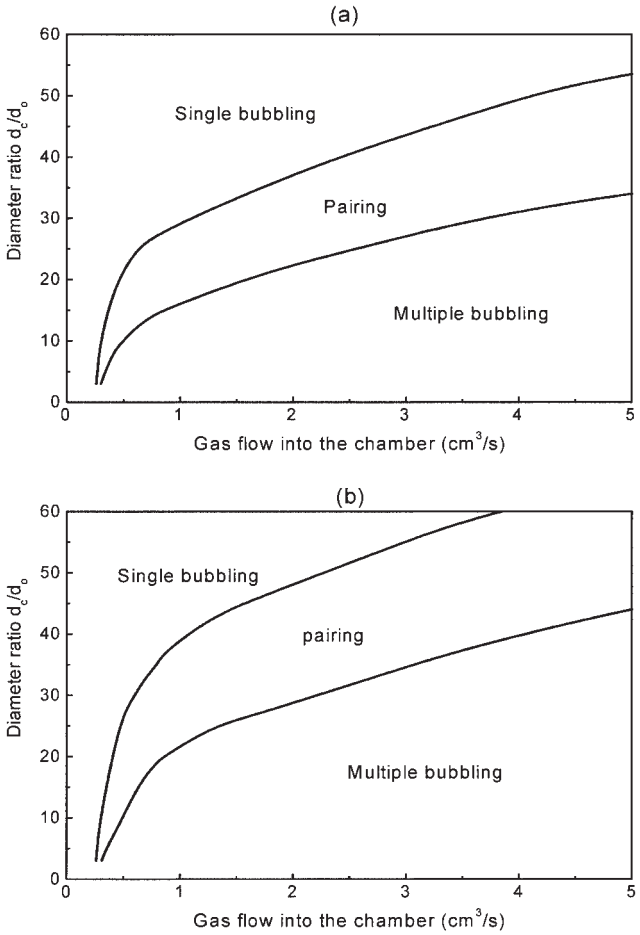

Figure 10. Model predictions of the regime map at (a) V_c = 430 cm^3 and (b) V_c = 1000 cm^3.

The corresponding bubbling frequencies for V_c = 1000 cm^3 are shown in Figures 9a, 9b, and 9c for orifice diameters 1.6, 2.0, and 2.4 mm, respectively. The experimental trends are similar to those in Figure 8, and again there is good agreement between theoretical predictions and experimental data.

Bubbling regime map

Theoretical regime maps predicted by our model are shown in Figures 10a and 10b for chamber volume V_c = 430 and 1000 cm^3, respectively, with gas flow and diameter ratio (d_c/d_o) as the parameters. Figure 10 shows boundaries between the three bubbling regimes described earlier: single bubbling, pairing, and multiple bubbling regimes. It is observed that with decreasing diameter ratio or increasing gas flow, the bubbling regimes generally transit from single bubbling to pairing and multiple bubbling. For the larger chamber volume, the boundaries between adjacent regimes are shifted upward significantly, in accord with our experimental findings.

At very low gas flow ($\lesssim$0.25 cm^3/s), the wall effect disappears because single bubbling occurs for all values of d_c/d_o. The bubble frequency (and thus bubble volume) is also independent of d_c/d_o, as can be seen in Figures 8 and 9. It appears that bubble–bubble interactions are negligible at low bubbling frequencies ($\lesssim$1 s^{-1}). For the case of single bubbling where bubble–bubble interactions are insignificant, the results obtained by the present model are very close to the rigorous solution using the boundary element method,[24] as outlined in the Appendix, which shows that the theoretical approach for the bubble–wall interaction in the present model is valid.

Conclusions

Our investigation demonstrates that the bubble–wall and bubble–bubble interactions can have a profound influence on bubbling frequencies and bubbling regimes in bubble formation at a submerged orifice. These effects have been successfully modeled by potential flow and bubble wake pressure analysis.

Notation

a = bubble radius, m
a_{sc} = radius of spherical-cap bubble, m
b = thickness of the plate, m
C_g = constant in Eq. 2, dimensionless
d_c = diameter of the bubble column, m
d_o = diameter of the orifice, m
f = bubble frequency, s^{-1}
f' = fanning friction factor, dimensionless
H = height of liquid above the orifice, m
k_o = orifice coefficient, dimensionless
N_{Re} = Reynolds number of detached rising bubble, dimensionless
P_a = gas pressure inlet to chamber, Pa
P_b = bubble pressure, Pa
P_c = chamber pressure, Pa
P_{cDET} = chamber pressure at bubble detachment, Pa
P_l = liquid pressure, Pa
$\bar{P}_l$ = average liquid pressure at bubble boundary, Pa
P_{or} = liquid pressure at the orifice, Pa
P_{st} = hydrostatic pressure at coordinate (r, θ), Pa
P_w = wake pressure, Pa
P_{wb} = wake pressure at the bubble surface, Pa
P_{wo} = wake pressure at the orifice, Pa
P_∞ = static pressure at the orifice, Pa
q = gas flow through the orifice, m^3/s
Q = gas flow into the chamber, m^3/s
r = radial coordinate, m
r_c = radius of the bubble column, m
r_o = radius of the orifice, m
Re_o = orifice Reynolds number defined in Eq. 2, dimensionless
s = perpendicular distance between bubble center and orifice, m
s_{bo} = distance between rising bubble and orifice, m
s_{bb} = mean distance between rising and growing bubble, m
t = time, s
t_f = bubble formation time, s
t_w = waiting time, s
T = time during waiting, s
u = velocity field of the liquid, m/s
u_o = instantaneous gas velocity through the orifice in Eq. 2, m/s
U = bubble vertical rising velocity, m/s
U_T = terminal rising velocity of spherical-cap bubble, m/s
V_b = bubble volume, m^3
V_c = chamber volume, m^3

Greek letters

γ = adiabatic exponent, dimensionless
θ = angular coordinate, rad
θ' = angle in Eq. 11, rad
μ_g = gas viscosity, kg m^{-1} s^{-1}
μ_l = liquid viscosity, kg m^{-1} s^{-1}
ρ_g = gas density, kg/m^3
ρ_l = liquid density, kg/m^3
σ = surface tension, N/m
ϕ = velocity potential, m^2/s

ϕ_p = velocity potential for expanding bubble, m^2/s
ϕ_T = velocity potential for translating bubble, m^2/s

Literature Cited

1. Collins R. The effect of a containing cylindrical boundary on the velocity of a large gas bubble in a liquid. *J Fluid Mech.* 1967;28:97-112.
2. Bhaga D, Weber ME. Bubbles in viscous liquids: Shape, wakes and velocities. *J Fluid Mech.* 1981;105:61-85.
3. Coutanceau M, Thizon P. Wall effect on the bubble behaviour in highly viscous liquids. *J Fluid Mech.* 1981;107:339-373.
4. Raebiger N, Vogelpohl A. Bubble formation in stagnant and flowing Newtonian liquids. *Ger Chem Eng.* 1982;5:314-323.
5. Raebiger N, Vogelpohl A. Calculation of bubble size in the bubble and jet regimes for stagnant and flowing Newtonian liquids. *Ger Chem Eng.* 1983;6:173-182.
6. Ruzicka MC, Drahoš J, Zahradnik J, Thomas NH. Structure of gas pressure signal at two-orifice bubbling from a common plenum. *Chem Eng Sci.* 2000;55:421-429.
7. Ruzicka MC, Drahoš J, Fialová M, Thomas NH. Effect of bubble column dimensions on flow regime transition. *Chem Eng Sci.* 2001; 56:6117-6124.
8. Davidson JF, Schüler BOG. Bubble formation at an orifice in an inviscid liquid. *Trans IChemE.* 1960;38:335-342.
9. Kupferberg A, Jameson GJ. Pressure behind a bubble accelerating from rest: Simple theory and applications. *Chem Eng Sci.* 1967;22: 1053-1055.
10. Kupferberg A, Jameson GJ. Bubble formation at a submerged orifice above a gas chamber of finite volume. *Trans IChemE.* 1969;47:241-250.
11. Zhang W, Tan RBH. A model for bubble formation and weeping at a submerged orifice. *Chem Eng Sci.* 2000;55:6243-6250.
12. Lamb H. *Hydrodynamics*. 6th Edition. Cambridge, UK: Cambridge Univ. Press; 1945.
13. Tan RBH, Harris IJ. A model for non-spherical bubble growth at a single orifice. *Chem Eng Sci.* 1986;41:3175-3182.
14. Miyahara T, Takahashi T. Bubble volume in single bubbling regime with weeping at a submerged orifice. *J Chem Eng Jpn.* 1984;17:597-602.
15. Tsuge H, Hibino S, Nojima U. Volume of a bubble formed at a single submerged orifice in a flowing liquid. *Int Chem Eng.* 1981;21:630-636.
16. Clift R, Grace JR, Weber ME. *Bubbles, Drops, and Particles.* New York, NY: Academic Press; 1978.
17. Mittoni LJ. *Deterministic Chaos in Metallurgical Gas–Liquid Injection Processes.* PhD Thesis. Melbourne, Australia: The University of Melbourne; 1997.
18. LaNauze RD, Harris IJ. Gas bubbles formation at elevated system pressures. *Trans IChemE.* 1974;52:337-348.
19. Milne-Thomson LM. *Theoretical Hydrodynamics*. 5th Edition. London, UK: Macmillan; 1968.
20. McCann DJ, Prince RGH. Regimes of bubbling at a submerged orifice. *Chem Eng Sci.* 1971;26:1505-1512.
21. Bonnet M. *Boundary Integral Equation Methods for Solids and Fluids.* Paris, France: Editions Eyrolles and CNRS Editions; 1995.
22. Power H. *BE Applications in Fluid Mechanics.* Southampton, UK: Computational Mechanics Publications; 1995.
23. Xiao ZY, Tan RBH. An improved model for bubble formation using the boundary-integral method. *Chem Eng Sci.* 2005;1:179-186.
24. Xiao ZY. *Bubble Formation and Bubble–Wall Interaction at a Submerged Orifice*. PhD Thesis. Singapore: National University of Singapore; 2004.

Appendix: Modeling of Wall Effect with the Boundary Integral Method

Boundary integral method

Over the past decades, the boundary integral method has received much attention from researchers and has became an important numerical technique in the computational solution of a number of physical problems. The method is based on Green's formula that enables the reformulation of the potential problem as the solution of a Fredholm integral equation, and some applications of this method are discussed by Bonnet[21] and Power.[22] Xiao and Tan[23] developed a theoretical model for bubble formation using a boundary integral method, and the details of the model development can be found in their paper.

The method is very briefly described here. First, the bubble surface is represented by n points, $(r_1, z_1), \ldots, (r_n, z_n)$, which divide the surface into $(n-1)$ elements. Then an isoparametric linear approximation is introduced to represent the surface and the velocity potential. With the collocation method, choosing these n points as collocation points yields n equations with the following form

$$2\pi\phi_i + \sum_{j=1}^{n-1} \int_{S_j} [(1-\xi)\phi_j + \xi\phi_{j+1}] \frac{\partial}{\partial n}\left(\frac{1}{|p_i - q_j|}\right) ds = \sum_{j=1}^{n-1} \int_{S_j} \left[(1-\xi)\frac{\partial \phi_j}{\partial n} + \xi \frac{\partial \phi_{j+1}}{\partial n}\right]\left(\frac{1}{|p_i - q_j|}\right) ds \quad (i = 1, \ldots, n) \quad \text{(A1)}$$

where ξ is the parameter in the range of (0, 1), p_i is the ith point with coordinates $p_i = (r_i, z_i, 0)$, and q_j is any point on the segment S_j with coordinates $q_j = [r(\xi), z(\xi), \theta]$.

After assembly, the set of equations has the following matrix structure

$$A\phi = B\frac{\partial \phi}{\partial n} \quad \text{(A2)}$$

where A and B are $n \times n$ matrices with the following values of items a_{ij} and b_{ij}

$$a_{ij} = 2\pi\delta_{ij} + \int_{S_j} (1-\xi)\frac{\partial}{\partial n}\left(\frac{1}{|p_i - q_j|}\right) ds + \int_{S_{j-1}} \xi \frac{\partial}{\partial n}\left(\frac{1}{|p_i - q_{j-1}|}\right) ds$$

$$b_{ij} = \int_{S_j} (1-\xi)\frac{1}{|p_i - q_j|} ds + \int_{S_{j-1}} \xi \frac{1}{|p_i - q_{j-1}|} ds \quad \text{(A3)}$$

With the values ϕ known on the bubble surface, the normal velocities $\partial\phi/\partial n$ at these collocation points are obtained by solving the matrix Eq. A2 with standard Gaussian elimination.

Method of images

To satisfy the no-flux boundary conditions on the rigid plane and impermeable column wall where the normal velocities are zero, a specific image system is introduced to account for the wall effect as shown in Figure A1. For this formulation, Green's function is further modified as

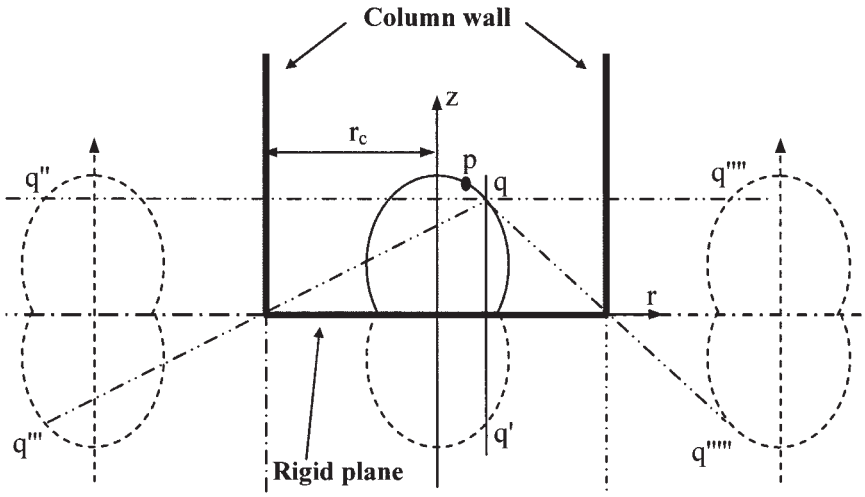

Figure A1. System of images.

$$G(p, q) = \frac{1}{|p - q|} + \frac{1}{|p - q'|} + \frac{1}{|p - q''|} + \frac{1}{|p - q'''|} + \frac{1}{|p - q''''|} + \frac{1}{|p - q'''''|} \quad \text{(A4)}$$

where q', q'', q''', q'''', and q''''' are the images of q as shown in Figure A1.

With the introduction of the image system, the model discussed in Xiao and Tan[23] can be further developed to take the wall effect into account on bubble formation. Although the model predicts the frequency well,[24] it unfortunately cannot predict the bubbling regime because of the lack of bubble–bubble interaction in the modeling.

Manuscript received Sep. 12, 2004, and revision received Jun. 22, 2005.